Interface Control Strategy of Synthesis LiMn$_2$O$_4$@Al$_2$O$_3$ Assisted by Tert-Butanol

*Yuhan Yao[1], Zhiwen Wang[1], Xiaohua Yu[1], Yingjie Zhang[1,2], Jianguo Duan[2], Chengyi Zhu[1], Zhitong Hu[1], Zhengjun Shen[1], Qiang Wang[1], Zhaolin Zhan[1], Peng Dong[2, *], Yannan Zhang[2, *],*

[1] National and Local Joint Engineering Laboratory for Lithium-ion Batteries and Materials Preparation Technology, Key Laboratory of Advanced Battery Materials of Yunnan Province, Faculty of Materials Science and Engineering, Kunming University of Science and Technology, Kunming 650093, China
[2] National and Local Joint Engineering Laboratory for Lithium-ion Batteries and Materials Preparation Technology, Key Laboratory of Advanced Battery Materials of Yunnan Province, Faculty of Metallurgical and Energy Engineering, Kunming University of Science and Technology, Kunming 650093, China
*E-mail: dongpeng2001@126.com (Peng Dong) zyn_legolas@163.com (Yannan Zhang)

LiMn$_2$O$_4$@Al$_2$O$_3$ cathode materials for lithium ion batteries are prepared through an sol-gel method with the assistance of tert-butanol. A uniform amorphous Al$_2$O$_3$ layer is formed on the surface of LiMn$_2$O$_4$ under the control of the hydrolysis mechanism of aluminum ion (Al^{3+}) and hydroxyl group (OH). The products are investigated by scanning electron microscopy (SEM), transmission electron microscopy (TEM), power X-ray diffraction (XRD), galvanostatic charge-discharge test system, electrochemical impedance spectroscopy(EIS) and inductively-coupled plasma emission spectrograph (ICP-AES). Structural and surface analysis reveal that the crystal structure and overall morphology of the LiMn$_2$O$_4$ electrode are found to be not significant unaffected by Al$_2$O$_3$ coating. Notably, the Al$_2$O$_3$-coating assistant by tert-butanol can produce a compact amorphous layer on the LiMn$_2$O$_4$ particles, and displays capacity losses of only 92.2% after 100 cycles at 55°C, which is much better than bare sample and the sample synthesized without the assistant of tert-butanol. Furthermore, EIS and ICP analyses show that the Al$_2$O$_3$ coating assisted by tert-butanol significantly improves the electro-conductivity and relieves the dissolution of Mn in electrolyte.

1. INTRODUCTION

Spinel LiMn$_2$O$_4$ is currently considered to be one of the most attractive cathode materials for rechargeable lithium-ion batteries due to its low cost, thermal safety, and excellent rate capability, compared with commercial LiCoO$_2$[1,2]. However, LiMn$_2$O$_4$ cathodes suffer from Jahn-Teller distortion

and manganese dissolution in the organic electrolyte, which corrupt the process ability and cyclic stability of LIBs at elevated temperatures. This is a tough issue to need be overcome [3,4]. Tremendous efforts have been made to enhance the electrochemistry performance of $LiMn_2O_4$. Surface coatings have been widely employed to reduce capacity fade in $LiMn_2O_4$, especially at elevated temperature condition [5]. Hence, formation of a stable interface is critical for improving cyclability and rate capacity of $LiMn_2O_4$ cathodes. It has been reported that amphoteric metal oxide coating, such as ZnO [6], $LiCoO_2$[7], Al_2O_3[8], MnO_2 [9], La_2O_3[10], and ZrO_2[11], is an effective route to prevent the direct contact of spinel $LiMn_2O_4$ with the electrolyte and inhibit Mn dissolution, thus resulting in improved cycles performance.

To our best knowledge, the uniformity and compactness of the coating substances have a critical impact on the performance of cathode materials especially for nanostructured battery electrodes [12,13]. It is regrettable that the limited promoting capability caused by limited self-structural stability for most traditional coating methods, which will limit the modification effect to some extent [14]. Therefore, it is highly necessary to explore novel modification techniques for realizing effective control of coating properties [15,16].

In this work, a low-cost additive (tert-butanol) was firstly introduced in the surface modification of $LiMn_2O_4$ with Al_2O_3. The hydroxyl group of tert-butanol molecular structure and the hydrogen bond among the aluminum salt easily formed a set of polymeric Al anchoring functional group on the $LiMn_2O_4$ core, which can effectively avoid cracking in the process of coating [17-19]. Thus, the interface controllable of $LiMn_2O_4@Al_2O_3$ cathode material can be realized. Furthermore, the influence of the Al_2O_3 coating synthesized with the assistant of tert-butanol on the crystal structure, particle morphology, electrochemical performances and the Mn^{2+} dissolution have also been investigated in detail.

2. EXPERIMENTAL

2.1 $LiMn_2O_4@Al_2O_3$ materials preparation

The pristine $LiMn_2O_4$ powder was prepared by MnO_2 (99.5% Aladdin) and $LiOH·H_2O$ (99.9%, Aladdin) at a molar ratio of 1:1.05, and dispersed into 5 mL pure ethanol to form a thick slurry, ground to form a fine mixture at agate mortar for 3 hours, and dried at room temperature, and calcining at 850°C for 12 h. The $LiMn_2O_4@Al_2O_3$ assistant by tert-butanol is synthesized by a sol-gel process. Stoichiometric aluminum sulfate octadecahydrate (99.9%, Aladdin) and sodium hydroxide (99.9%, Aladdin) were completely dissolved in 200 mL absolute ethanol, then, the $LiMn_2O_4$ powder and tert-butanol (mass ratio $LiMn_2O_4$: tert-butanol =100:5) were slowly added into the solution with the continue stirring for 4 h at 55°C, following by heating in air at 100°C. Finally, the obtained powder was sintered at 600 °C for 5 h to obtain the $LiMn_2O_4@Al_2O_3$ sample. The pristine $LiMn_2O_4$ and $LiMn_2O_4@Al_2O_3$ samples without/with the assistant of tert-butanol were cited as LMO, ALMO, and TALMO, respectively, and the coating amount of Al_2O_3 was 2 wt.% of the pristine $LiMn_2O_4$ powder.

2.2 Analytical methods

High temperature aging investigations of the samples were done by keeping 300 mg powder sample with 20 cm^3 selected electrolyte (1 M LiPF$_6$ in 1:1:1 ethyl methyl carbonate + ethylene carbonate + dimethyl carbonate in volume) in a sealed Teflon container for 10 and 20 days at 55 °C. After electrolyte was separated from the powders by centrifugation, the content of dissolved manganese in the electrolyte was determined by ICP analysis using IRIS Intrepid II XSP inductively coupled plasma-atomic emission spectrometer (ICP-AES). The surfaces of electrodes, fresh and cycled, and LMO, ALMO, and TALMO powders, fresh and stored in the presence of electrolyte, were investigated. Cycled electrodes were extracted from cells in an Ar glove box after activation, 100 cycles, rinsed with DMC and dried overnight. The fresh electrodes were not exposed to electrolyte. The X-ray diffraction (XRD, Rigaku, Japan) was performed with Cu-K_α radiation (1.5418 Å) at 40 kV, 150 mA with a scanning speed of 2°/min. The morphology and particle size estimation of samples were tested by scanning electron microscope (SEM, TESCAN VEGA3, CZE). Transition electron microscope (TEM, JEM-2010, Japan) was employed for microstructure and morphology analysis. we're following our previous report [20]. The cathode material consisted of 80 wt.% of LMO, ALMO, and TALMO, 10 wt.% of the conductive carbon black (Super P), and 10 wt.% of polyvinylidene fluoride, which were thoroughly mixed and bonded with Nmethyl-2-pyrrolidinone solvent. The average mass loading of LLMO materials on the electrode was 1.51 mg cm^{-2}. Lithium metal sheet and Celgard 2300 film were selected as anode and separator, respectively. The electrolyte solution was composed of 1M LiPF$_6$ in ethylene carbonate, ethyl methyl carbonate, and dimethyl carbonate in a volume ratio of 1:1:1.

To evaluate the electrochemical performance, charge-discharge tests were carried out at different current densities in a voltage range of 2.5-4.6 V with a LAND-CT2001A test system. The electrochemical impedance spectroscopy (EIS) property of the as prepared samples were also tested by same electrochemical workstation (CHI660D, Shanghai, China). The impedance spectra were recorded potentiostatically by applying an ac voltage of 5 mV amplitude over the frequency range from 10^5 to 0.01 Hz after the cells (after desired cycles) were left at the full charged state for 10 h to achieve equilibrium.

3. RESULTS AND DISCUSSION

3.1. Structural and morphological characterization

Fig. 1 displays the XRD patterns of pristine LMO, ALMO and TALMO samples. As can be seen from the figure, all the diffraction peaks are assigned to a Fd-3m space group identical and can be indexed to standard card (JCPDS: 35-0782) [21, 22]. No diffraction peaks of Al$_2$O$_3$ or other impurity phases are discovered in the XRD pattern of LiMn$_2$O$_4$@Al$_2$O$_3$ samples, Moreover, the lattice constants of LMO and LMO-coated are 8.2210Å, 8.2213 Å and 8.2212 Å, which is calculated by Jade 6.0 software. It suggests that the distribution of aluminum in LiMn$_2$O$_4$@Al$_2$O$_3$ has no remarkably effect on the spinel natural structure of LiMn$_2$O$_4$ based material.
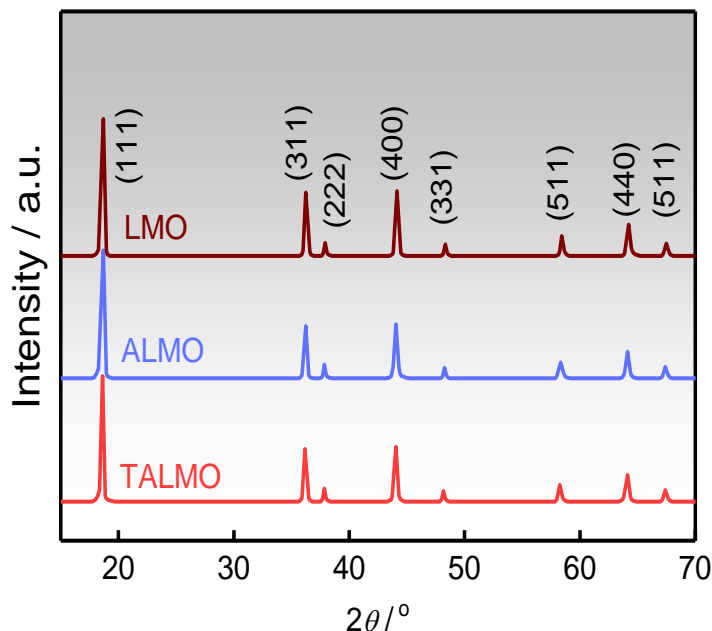
Figure 1. XRD patterns of the pristine LMO, ALMO and TALMO samples.

SEM and TEM are used for characterized the morphology and structure of as prepared active powders. Fig. 2 (a-c) present SEM images of LMO, ALMO and TALMO, respectively. It can be clearly seen that the pristine LMO particles displays a high crystallized structure with a primary size of about 100-200 nm (Fig. 2 (a)), and the other two coated samples have the same s morphology. Notably, the tert-butanol assisted Al_2O_3 coated sample TALMO displays an armor-like surface when compared with the ALMO samples, indicating that the coating layers are more compact after tert-butanol assisted modification.
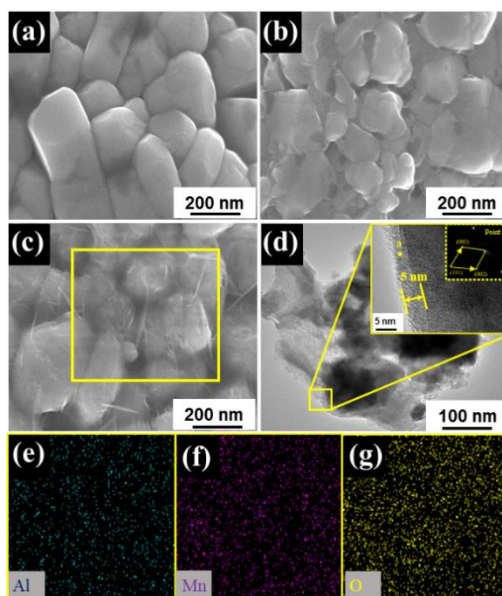
Figure 2. SEM image of LMO (a), ALMO (b) and TALMO (c), TEM images of TALMO (d) and EDS images (e, f, g) of TALMO.

EDS elemental mapping of Al, Mn and O (Fig. 2 (e-g)) for the tert-butanol assisted Al_2O_3 coated Li_2MnO_4 reveals that these elements are distributed in the particles homogeneously. The Al_2O_3 based shell can also be well confirmed by TEM results, as shown in Fig. 2(d), there is a distinct interface with a thickness of approximately 5 nm is formed on the surface of crystalline LMO. In addition, according to the selected-area electron diffraction (SAED) observation, the amorphous coating layer consists of (111) and (002) planes, corresponding to the standard diffraction of Al_2O_3 (JCPDS#88-0107) [23]. In a word, the tert-butanol assisted Al_2O_3 coated $LiMn_2O_4$ has been demonstrated roundly by SEM, EDS and TEM measurements.

3.2 Electrochemical performance

Fig. 3 summarizes the cycles performances of pristine LMO and Al_2O_3-coated LMO with / without the of tert-butanol at 55°C with 0.2 C rate in a voltage range of 3.0–4.3 V versus Li/Li^+. It can be seen from Fig. 3 that the LMO displays a bit higher initial discharge capacity (114.69 mAh g^{-1}) than ALMO (108.43 mAh g^{-1}) and TALMO (105.46 mAh g^{-1})，because Al_2O_3 is electrochemically inactive at 3.0–4.2 V versus Li^+/Li, and mass of active material per unit area on the electrode is also reduced, leading to decreasing of the initial capacity [24,25]. Interestingly, the discharge capacity of LMO decreases sharply after 100 cycles at 55°C, which is mainly due to the structure degradation accelerated by the side reaction between electrode and electrolyte. This phenomenon however can be effectively enhanced by tert-butanol assisted Al_2O_3 coating. The discharge capacity of TALMO decrease to 95.73 mAh g^{-1} displaying a capacity fades of only 9.22%, which is significantly improved compared with pristine LMO (34.11%%) and ALMO (15.03%), indicating that the Al_2O_3 coating synthesized with the assistance of tert-butanol can availably enhances the structural stability and avert the erosion of electrolyte, due to the stubborn surface.
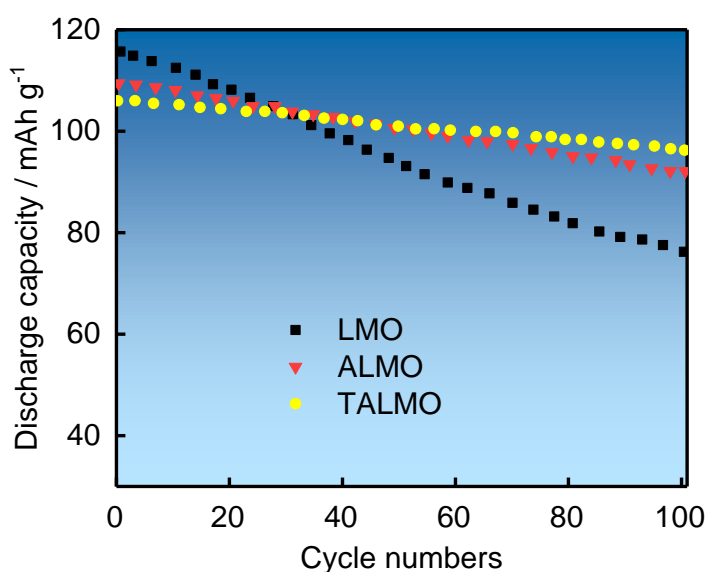
Figure 3. Cycles performance of the LMO, ALMO and TALMO at 55°C and a 0.2 C charge/discharge rate

To further investigate the rate performance of all three samples, the charge / discharge cycle testing was tested at 55°C with different charge and discharge current. As shown in Fig. 4, the Al_2O_3 coated LMO with the assistance of tert-butanol exhibits a superior rate performance than pristine LMO and ALMO at 1, 3 and 5 C current rate, especially at 3 C and 5 C. After 40 cycles, the capacity retention of TALMO is 92.36%, much better than the uncoated material (72.76%). This improvement of rate capability is mainly attributed to the coated Al_2O_3 layer which provides ion diffusion channels on the surface of $LiMn_2O_4$ electrode with better ionic conductivity [26, 27]. The capacity relation of TALMO is also improved than the ALMO (81.60%), because the hydroxyl group of tert-butanol molecular structure and the hydrogen bond among the aluminum salt may easily produce a set of polymeric Al anchoring functional group on the $LiMn_2O_4$ core, which can effectively form a compact Al_2O_3 armor and avoid layer cracking in the process of coating.
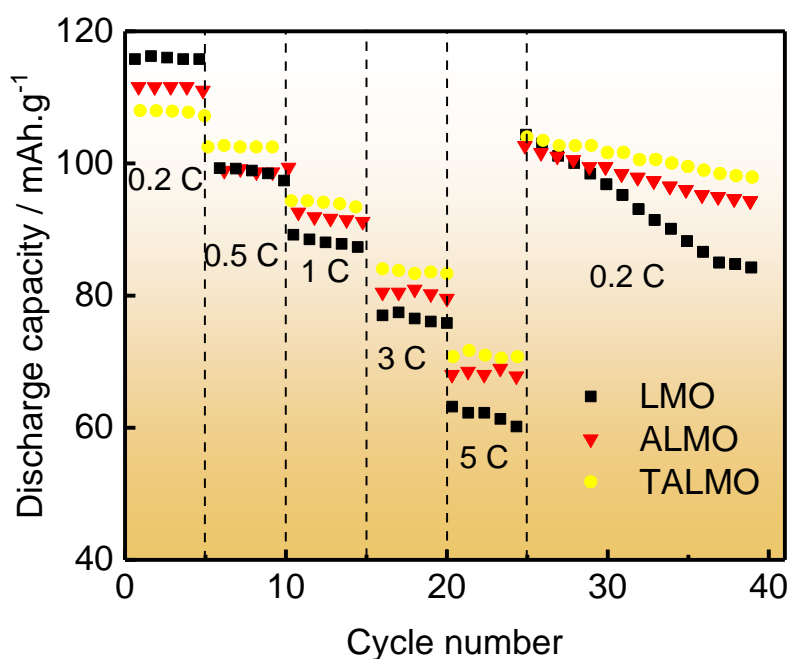
Figure 4. Rate capability of LMO, ALMO and TALMO

EIS is also applied to further discuss the reason for the upgrade of the cycles performance of the $LiMn_2O_4@Al_2O_3$ electrode. Fig 5 displays the EIS plots of LMO, ALMO and TALMO cells after 100 cycle. The AC impedance spectrum consist of two parts. The semicircle in the high frequency reflects the migration resistance and charge transfer resistance of Li^+ in the SEI film, the oblique line in the low frequency region reflects the Warburg impedance (Zw) caused by the diffusion of lithium ions inside the positive electrode material [28]. Z-view software is involved for fitting the corresponding equivalent circuit model (Fig. 5a insert), where R_s, R_f, and R_{ct} are the diffusion resistance of Li^+ in the electrolyte, the resistance of the SEI membrane covering the electrode surface, and the charge transfer impedance of the electrode reaction，respectively [29, 30].

As can be seen from Fig.5a, the film resistances (R_f) of ALMO and ATLMO are slightly greater than the film resistance (R_f) of pristine LMO at the 1st cycle, mainly because the SEI and Al_2O_3 coating layer formed on the surface of the cathodes. After 100 cycles, the charge transfer resistance (R_{ct}) of

ALMO and TALMO is 286.32 Ω and 163.51 Ω, much lower than the R_{ct} of pristine LMO (637.62 Ω), which is attributed to the protective Al_2O_3 coating layers prevent the occurrence of side reactions (as shown in Table 1), resulting the significant decrease in R_{ct} for the Al_2O_3 coated LMO[31,32].This indicates that the Al_2O_3 coating assisted by tert-butanol can produce a favorable interface on the surface of pristine $LiMn_2O_4$ for lithium ion transport. This is consistent with the previous results of electrochemical performance.
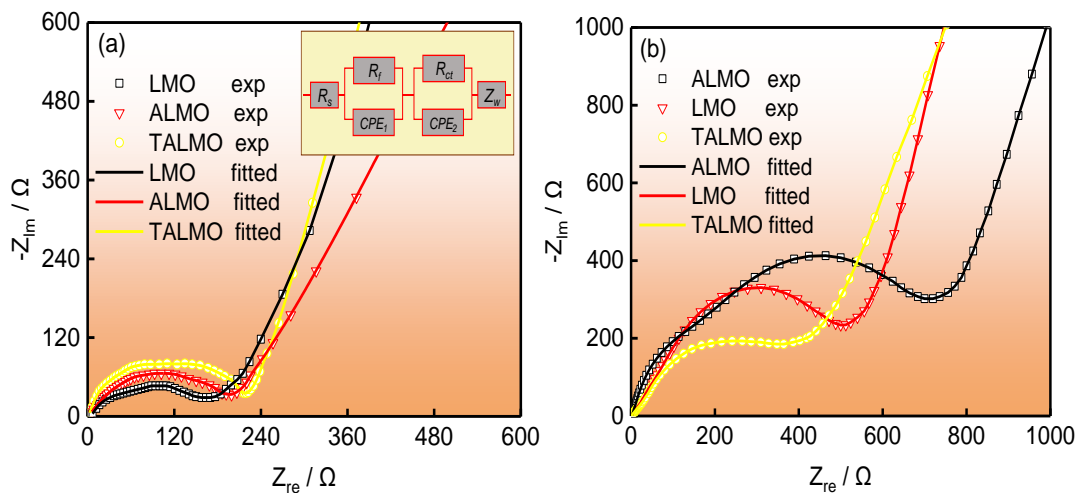
Figure 5. AC impedance spectroscopy and equivalent circuit diagram of samples at the 1st cycle and 100th cycle.

Table 1. The fitted combined impendence resistance of pristine LMO, ALMO and TALMO after 100th cycles at 0.2 C.

Sample	LMO	ALMO	TALMO
R_s / Ω	3.56	3.29	2.61
R_f / Ω	39.12	36.53	26.71
R_{ct} / Ω	637.62	286.32	163.51

According to Oliveira's [33] research, the loss of discharge capacity is mainly attributed to the degradation of LMO particles with the Mn concentrations at elevated temperature. To further prove the phenomenon, the various uncoated and coated samples stored in electrolyte at 55°C were subjected to ICP testing for Mn dissolution, the results are displayed in Fig. 6. Interestingly, the discharge capacity of LMO decreases sharply after 100 cycles at 55ºC, which is mainly due to the Mn dissolution is accelerated by the side reaction between electrode and electrolyte" To clarify whether or not surface modification will affect the dissolution of Mn (as show Fig. 6), the aging experiment was carried out at 55 °C for 10 days, 20 days [34, 35], and the amount of dissolved Mn in the electrolyte were analyzed. After storage for 20 days, the Mn dissolution of pristine LMO, ALMO, and TALMO are 218.5 ppm, 96.7 ppm and 62.3 ppm, respectively. Compared with the sample of pristine LMO and ALMO, the sample of TALMO exhibits the minimum amount of Mn in the electrolyte. This indicates that the Al_2O_3

coating assisted with TBA can significantly reduce the manganese dissolution at elevated temperatures and restrain the side reactions on the spinel $LiMn_2O_4$ surface, thereby enhancing the electrochemical performances.
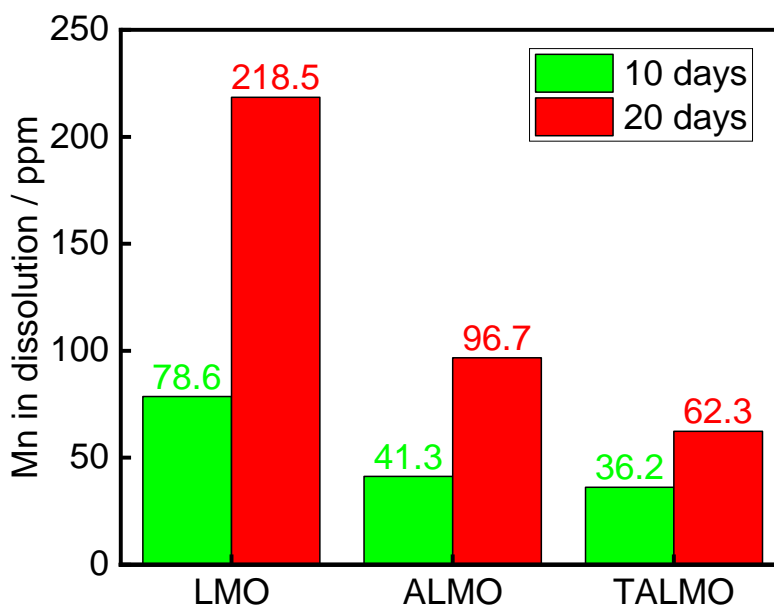
Figure 6. Relation of storage time and Mn dissolution for different samples at 55°C.

The SEM images of the cycled electrodes is carried out for monitoring the effect of polymeric Al anchoring functional group on the stability of the spinel structure. Fig. 7 (a-c) displays the SEM image of the cycled electrodes for LMO, ALMO, and TALMO after 100 cycles at 1C, respectively. Compared with the sample of TALMO (Fig. 7 (c)), a large crack is observed on the surface of the LMO and ALMO electrode after 100 cycles, along with a crack on the particle of the active materials in the inset, which results from the electrolyte erosion and inferior structural stability. However, the TALMO does not show the development cracks after 100 cycles, as show in Fig. 7 (c). This demonstrates that Al anchoring functional group acts as a protective layer to suppress the electrolyte erosion and keep the structural stability, giving rise to the improved cycles performance.
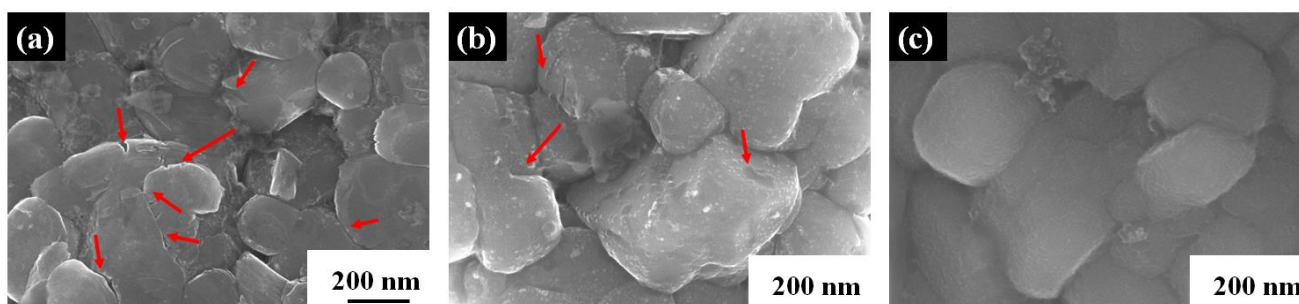
Figure 7. SEM image of the anode after 100 cycles, (a) LMO, (b) ALMO, and (c) TALMO

4. CONCLUSION

In summary, we had successfully prepared a compact and uniform Al_2O_3 coating layer on the surface of LMO with the assistance of tert-butanol via a facile sol-gel method. A compact amorphous Al_2O_3 skin on spinel $LiMn_2O_4$ core inhabits the side reactions during cycles by separating the electrode from the electrolyte directly, which has been confirmed by SEM, TEM, EDS, EIS and ICP clearly. Electrochemical analysis reveals that the tert-butanol assisted coated sample exhibits an excellent cycles performance and the favorable capacity retention of 90.78% after 100 cycles at 55°C, which is much better than the pristine LMO and the Al_2O_3-coated sample without the assistance of tert-butanol. This because the hydroxyl group of tert-butanol molecular structure and the hydrogen bond among the aluminum salt may easily produce a set of polymeric Al anchoring functional group on the $LiMn_2O_4$ core, which can effectively form a compact Al_2O_3 armor and avoid layer cracking in the process of cycles.

References

1. D.J. Guo, C.Y. Bing, J.J. Bing, D. Ke, P,Z. Dong, H.G. Rong, *J. Power Sources*, 268 (2014) 146.
2. M. Zhao, X. Song, F. Wang, W. Dai, X. Lu, *Electrochim. Acta*, 56 (2011) 5673.
3. Y.N. Zhang, Y.Y. Zhang, Y.J. Zhang, P. Dong, Q. Meng, M.L. Xu, *J. Alloy. Compd.*, 209 (2019), 225-234.
4. T, Arture, Y. D. Park, J. Mun, *J. Power Sources*, 325 (2016) 360.
5. K. F. Cheng, H.M. Wang, Z.W. Zhu, M. Wang, T.J. Zhang, Z.L. Tao, J. Chen. *Energy Environ. Sci.*, 4 (2011) 3668.
6. J.X. Dong, Y.Z. Tao, L.J. Xiong, D. Peng, Z. Y. Jie, Y.Y. Han, C. Qi, L. Cheng, Z. Y. Nan, Y.X. Hua, *Int. J. Electrochem. Sci.*, 13 (2018) 2167.
7. L.X. Ning, G.D. Sheng, W. Ying, J. *Nanosci. Nanotechno.*, 12 (2012) 7113.
8. Z.Y. Nan, D. Peng, Y.X. Hua, X.S. Biao, Y.R. Ming, L.H. Xin, S.Z. Zhong, Y. Yao, L. Xue, Z.Y. Jie. *Int. J. Electrochem. Sci.*, 12 (2017) 6853.
9. A.M. Kannan, A. Manthiram, Electrochem. Solid ST., 5 (2002) 167.
10. Z.Y. Nan, D. Peng, Z.M. Yu, S.X. Liang, Y.X. Hua, S.J. Jie, M. Qi, L. Xue, Z.Y. Jie. *J. Appl. Electrochem.*, 48 (2018) 135.
11. W.K. Kim, D.W. Han, W.H. Ryu, S.J. Lim, H.S. Kwon, *Electrochim. Acta*, 71 (2012) 1721.
12. S.T. Mung, K. Zumi, S. Komaba, Y.K. Sun, H.Yashiro, N. Kumagai, *Chem. Mater.*, 17 (2005) 3695.
13. L.X. Hui, K.L. Qin, S. Ting, L. Kun, C. Li, J. Power Sources, 267 (2014) 874.
14. A.M. Hashem, A.E. Abdel, H.M. Abuzeid, R.S. Tawil, S. Indris, H. Ehrenberg, A. Mauger, C.M. Julien, *J. Alloy Compd.*, 737 (2018) 758.
15. B. Ying, W. Chuan, W. Feng, W. Borong, C. Shi, *Mater. Sci. Forum*, 676 (2011) 37.
16. L.J. Xiong, J.X. Dong, Z.Y. Nan, D. Peng, D.J. Guo, Z.Y. Jie, L.Y. Feng, F.Z. Wei, Y.Y. Han, Z.C. Yi, Y.X. Hua, Z.Z. Lin, *Int. J. Electrochem. Sci.*, 13 (2018) 1352.
17. J. C. Ray, K. S. You, J. W. Ahn, W. S. Ahn, *Micropor. Mesopor. Mat.*, 100 (2007) 183-190.
18. H. C. Lee, H. J. Kim, C. H. Rhee, K. H. Lee, J. S. Lee, S. H Chung, *Micropor. Mesopor. Mat.*, 79

(2005), 61-68.

19. S. Bi, C. Wang, Q. Cao, C. Zhang, *Coordin. Chem. Rev.*, 248 (2004), 441-455.
20. G. D. Sheng, A. Judith, W. Ying, *Nanoscal*, 3 (2011) 1465.
21. Y.N. Zhang, P. Dong, M.Y. Zhang, X.L. Sun, X.H. Yu, J.J. Song, Q. Meng, X. Li, Y.J. Zhang, *J. Appl. Electrochem.*, 48(2018), 135-145.
22. Z.Y, Nan, Z.Y. Jie, Z.M. Yu, X.M. Li, L. Xue, Y.X. Hua, D. Peng. *JOM*, 5 (2018) 1007.
23. Y. Shuo, D.O. Schmidt, A. Khetan, F. Schrader, S. Jakobi, M. Homberger, M. Noyong, A. Paulus, H. Kungl, *Materials*, 11 (2018) 806.
24. T.K. Fey, P. Muralidharan, L.C. Zhang, Y.D. Cho, *Electrochim. Acta*, 51 (2006) 4850.
25. K.S. Fei, Q.H. Fei, F. Yao, L. Xi, W.Y. Gang, *Electrochim. Acta*, 144 (2014) 22.
26. R. H. French, *J. Am. Ceram. Soc.*, *73*(1990), 477-489.
27. A. Peters, C. Korte, D. Hesse, N. Zakharov, J. Janek, *Solid State Ionics*, 178 (2007), 67-76.
28. C.Y. Ouyang, X.M. Zeng, Z. Sljivancanin, A. Baldereschi, *J. Phys. Chem. C*, 114 (2010) 4756.
29. G.D. Sheng, W.Ying, *Ionics*, 19 (2012) 1.
30. W.Z. Wen, D.R. Jia, Y.X. Hua, F.T. Lin, Z. Yan, Z.Z. Lin. *Int. J. Electrochem. Sci.*, 13 (2018) 4411.
31. G.H. Waller, P.D. Brooke, B.H. Rainwater, S.Y. Lai, R. Hu, S.Y. Lai, D. Ying, F.M. Alamg, K.H. Sandhage, M.L. Liu, *J. Power Sources*, 306 (2016) 162.
32. Z.R. Rui, L.J. Xing, H.J. Jun, Z.R. Yu, Z.J. Feng, C.H. Yu, S. Guang, *J. Alloys Compd.*, 724 (2017) 1109.
33. N.T.C. Oliveira, A.C. Guastaldi. *Acta Biomater*, 5 (2009) 399.
34. J. Tu, X. B. Zhao, G. S. Cao, D. G. Zhuang, T. J. Zhu, J. P. Tu, *Electrochim. Acta*, *51* (2006), 6456-6462.
35. K. Yamagiwa, D. Morita, N. Yabuuchi, T. Tanaka, M. Fukunishi, T. Taki, Y. T. Cui, *Electrochim. Acta,*, 160 (2015), 347-356.